Parallel Spin-Wave Pumping in Yttrium Garnet Single Crystals

V. V. Zautkin, V. E. Zakharov, V. S. L'vov, S. L. Musher, and S. S. Starobinets
Computation Center, Siberian Division, USSR Academy of Sciences
Submitted October 6, 1971
Zh. Eksp. Teor. Fiz. 62, 1782–1797 (May, 1972)

The behavior of spin waves beyond the parametric excitation threshold is considered theoretically and experimentally and with an electronic computer for the particular case of parallel pumping in yttrium garnet (YIG). It is shown that the previously developed nonlinear stationary theory of parametric excitation of waves is in good qualitative and quantitative agreement with the experiments. The theory was compared with the experimental values of the real and imaginary parts of the stationary nonlinear susceptibility χ' and χ'', with the sign of χ', dependence of χ' and χ'' on power level in YIG samples of different shapes in various magnetic fields.

THE problem of the nonlinear behavior of waves that 1 are parametrically excited by a spatially-homogeneous field was investigated in general form (for media for which the classical Hamiltonian formalism can be introduced) in our preceding papers[1,2]. It was shown there at not too large amplitudes of the homogeneous field the Hamiltonian of the wave system can be simplified and taken in the form

$$H=\sum_{\mathbf{k}}\left(\omega_{\mathbf{k}}+\sum_{\mathbf{k}'}T_{\mathbf{k}\mathbf{k}'}a_{\mathbf{k}'}a_{\mathbf{k}'}^{*}\right)a_{\mathbf{k}}^{*}a_{-\mathbf{k}}^{*}+{}^{1}/_{2}\sum_{\mathbf{k}}\left\{\left((h(t)V_{\mathbf{k}}+\sum_{\mathbf{k}'}S_{\mathbf{k}\mathbf{k}'}a_{\mathbf{k}'}a_{-\mathbf{k}'}\right)a_{\mathbf{k}}^{*}a_{-\mathbf{k}}^{*}+\text{c.c.}\right\}. \tag{1}$$

Here $a_{\mathbf{k}}$ are the complex amplitudes of the waves, $\omega_{\mathbf{k}}$ their dispersion law, $h(t) = h\exp(-i\omega_p t)$ and $V_{\mathbf{k}}$ are the amplitude of the homogeneous field and the coefficient of coupling with it, and $S_{\mathbf{k}\mathbf{k}'}$ and $T_{\mathbf{k}\mathbf{k}'}$ are the nonlinear characteristics of the medium. Such a choice of the Hamiltonian corresponds to allowance for only the self-consistent interaction of a pair of waves with equal and opposite wave vectors. The theory based on this approximation (which we shall henceforth call the S-theory, for brevity) makes it possible to analyze in detail the picture of the behavior of the parametrically-excited waves beyond the threshold.

We present here the results of an experimental study of the excitation spin waves in yttrium garnet (YIG) single crystals by the parallel-pumping method (Sec. 3). Single-crystal yttrium garnets have a "high Q" ($\gamma/\omega \sim 10^{-4}$) contain a minimum of impurities and defects, so that the experimental results can be compared with the predictions of the theory. To effect such a comparison, we need a more detailed extension of the S-theory to include the concrete case of parametric excitation of spin waves in an isotropic ferromagnet, such as the yttrium garnet is in the first approximation (Sec. 1). We calculated the coefficients $S_{\mathbf{k}\mathbf{k}'}$ and $T_{\mathbf{k}\mathbf{k}'}$ for an isotropic ferromagnet, with allowance for the exchange, dipole-dipole, and Zeeman interactions (Appendix 1). These coefficients were used later to calculate the stationary distributions of the spin waves in k-space, the nonlinear high-frequency susceptibilities χ' and χ'' of the crystal, and also to calculate the transient regime. These calculations can be carried out analytically only in the simplest cases, and computer calculations were made for an extensive comparison of the S-theory with experiment (Sec. 2). The comparison of the calculated behavior of the susceptibilities χ' and χ'' (as functions of the high-frequency field amplitude) with those observed experimentally for samples of different shapes confirms the main qualitative conclusions of the S-theory and is in satisfactory quantitative agreement with it (Sec. 4). In particular, it confirms the conclusion that at not too large excesses above the threshold of the parametric instability the spin waves lie in k-space on the "equator" of the surface $\omega_{\mathbf{k}} + 2\Sigma T_{\mathbf{k}\mathbf{k}'}n_{\mathbf{k}'} = 0$, in a plane perpendicular to the magnetization direction, and also the conclusion that the spin waves are excited stage by stage on discrete "latitudes" of this surface at large field amplitudes. The stage-by-stage excitation was verified also by direct experiment. The role of the factors not accounted for by the S-theory (nonlinear damping, inhomogeneities, etc) is discussed in the Conclusion.

1. S-THEORY FOR ISOTROPIC FERROMAGNETS

The equations for the amplitudes $a_{\mathbf{k}}$ should be obtained within the framework of the S-theory by varying the Hamiltonian (1):

$$\frac{\partial a_{\mathbf{k}}}{\partial t}+\gamma_{\mathbf{k}}a_{\mathbf{k}}=-i\frac{\delta H}{\delta a_{\mathbf{k}}^{*}}. \tag{2}$$

The wave damping $\gamma_{\mathbf{k}}a_{\mathbf{k}}$ is introduced in these equations phenomenologically. Expanding (2) and changing over to the variables $n_{\mathbf{k}} = a_{\mathbf{k}}a_{\mathbf{k}}^{*}$, $\sigma_{\mathbf{k}} = a_{\mathbf{k}}a_{-\mathbf{k}}e^{i\omega_p t} = n_{\mathbf{k}}e^{i\psi}_{\mathbf{k}}$, we obtain

$$\frac{1}{2}\frac{dn_{\mathbf{k}}}{dt}=n_{\mathbf{k}}\{-\gamma_{\mathbf{k}}+\operatorname{Im}(P_{\mathbf{k}}^{*}e^{i\psi_{\mathbf{k}}})\},$$
$$\frac{1}{2}\frac{d\psi_{\mathbf{k}}}{dt}=\tilde{\omega}_{\mathbf{k}}+\operatorname{Re}(P_{\mathbf{k}}^{*}e^{i\psi_{\mathbf{k}}})\}. \tag{3}$$

Here

$$\tilde{\omega}_{\mathbf{k}}=\omega_{\mathbf{k}}-\omega_{p}/2+2\sum_{\mathbf{k}'}T_{\mathbf{k}\mathbf{k}'}n_{\mathbf{k}'} \tag{4}$$

is the renormalized wave dispersion law, and

$$P_{\mathbf{k}}=hV_{\mathbf{k}}+\sum_{\mathbf{k}'}S_{\mathbf{k}\mathbf{k}'}n_{\mathbf{k}'}e^{i\psi_{\mathbf{k}'}} \tag{5}$$

is the self-consistent pumping renormalized to take into account the interaction between pairs. This renormalization is the main mechanism that leads to a limitation on the spin-wave amplitudes[3].

As shown in[1], in the stationary state the spin waves are distributed in k-space on the surface $\tilde{\omega}_{\mathbf{k}} = 0$. This distribution can be singular (in the form of individual

points, lines, etc). For those surface points at which the spin-wave amplitude differs from zero, it follows from (3) that

$$P_k + i\gamma_k e^{i\psi_k} = 0. \tag{6}$$

In this case $|P_k| = \gamma_k$. On the remaining surface

$$|P_k| < \gamma_k. \tag{7}$$

The conditions (6) and (7) determine uniquely the distribution of the spin waves on the surface $\tilde{\omega}_k = 0$.

For an isotropic ferromagnet, the problem has axial symmetry about the direction of the magnetization M. We introduce the polar and azimuthal angles θ and φ. Then (see[4])

$$V_k = -\frac{g\omega_M}{\omega_p}\sin^2\theta e^{2i\varphi} = V(\theta)e^{2i\varphi}.$$

Here g is the gyromagnetic ratio, $\omega_M = 4\pi g M_0$, M_0 is the magnetization, and the coefficient $S_{kk'}$ on the surface is given by $S_{kk'} = S(\theta, \theta'; \varphi - \varphi')$. We average (6) over the angle φ'_k, introducing $\psi_\theta = \psi_k - 2\varphi$, $N_\theta = \int_0^{2\pi} n(\theta, \varphi)d\varphi$,

$$S(\theta,\theta') = \frac{1}{2\pi}\int_0^{2\pi} S(\theta,\theta',\varphi-\varphi')e^{-2i(\varphi-\varphi')}d(\varphi-\varphi'). \tag{8}$$

we obtain

$$hV_\theta + \sum_{\theta'} S(\theta,\theta')N_{\theta'}\exp i\psi_{\theta'} + i\gamma_\theta \exp i\psi_\theta = 0. \tag{9}$$

The empirical $\gamma(\theta)$ dependence for isotropic ferromagnets is given by[5]

$$\gamma(\theta) = (1 + 2\sin^2 2\theta)\gamma_0. \tag{10}$$

The threshold of the parametric excitation is defined by the condition

$$h_1 = \min(\gamma(\theta)/V(\theta)).$$

The minimum is realized for $\theta = \pi/2$, so that at $h \approx h_1$ the wave-excitation conditions are satisfied only for $\theta \approx \pi/2$.

The requirement $|P| \leq \gamma$ allows us to prove (see[1]) that in the nonlinear regime at $h \sim h_1$ there will be excited only one group of waves with $\theta = \pi/2$, amplitude N_1, and phase ψ_1. Here, as seen from (9),

$$N_1 = \frac{[(hV_1)^2 - \gamma^2]^{1/2}}{|S_{11}|}, \quad \sin\psi_1 = \frac{\gamma}{hV_1}, \quad \cos\psi_1 = -\frac{S_{11}N_1}{hV_1}, \tag{11}$$
$$V_1 = V(\pi/2), \qquad S_{11} = S(\pi/2, \pi/2).$$

It follows from symmetry considerations that

$$P_k = P(\theta)\exp(2i\varphi_k).$$

If one group of waves is excited, then

$$P(\theta) = hV(\theta) + S_{\theta_1}N_1 e^{i\psi_1}, \qquad S_{\theta_1} = S(\theta, \pi/2). \tag{12}$$

It is easy to verify with (11) and (12) that at $h \gtrsim h_1$ we get $|P(\theta)| < \gamma(\theta)$ if $\theta \neq \pi/2$. This condition is violated if $|P(\theta) = \gamma(\theta)$ at $\theta \neq \pi/2$, which yields for the threshold h_2 of production of the second pair of waves (see[1])

$$h_2^2 = \min\left\{h_1^2 + \frac{h_1^2 S_{11}^2(\gamma_\theta^2 V_1^2 - \gamma_1^2 V_\theta^2)}{\gamma_1^2(S_{\theta_1}V_1 - V_\theta S_{11})^2}\right\}$$

At small $\theta - \theta_1$, the expression in the curly brackets behaves like $(\theta - \theta_1)^{-2}$, and therefore the second group of pairs cannot occur close to the first group; at $h = h_2$ the second group occurs at a "latitude" $\theta_1 - \theta_2 \sim 1$. This conclusion is an important consequence of the S-theory.

To estimate the threshold h_2 and the angle θ_2, we made in[1] the very simple assumptions $\gamma_\theta = \gamma_1$ and $S_{\theta_1} = S_{11}$. Then $h_2^2/h_1^2 = 2$ and $\theta_2 = 0$. This estimate, however, is too crude. Indeed, it is seen from (8) that $S_{\theta_1} = 0$ from symmetry considerations. We assume the approximation $\gamma_\theta = \gamma_1$ and

$$S_{\theta_1} = S_1\sin^2\theta + S_2\sin^4\theta. \tag{13}$$

Then

$$h_2^2/h_1^2 \approx 1 + 11(S_1/S_2 + 1)^2.$$

Even if $S_2 \sim S_1$, the threshold for the production of the second group of pairs is ~ 10 dB. It is curious that in the approximation (13) the angle θ_2 does not depend on the ratio of S_1 and S_2:

$$\theta_2 = \arcsin(1/2\sqrt{5} - 1) \approx 51°.$$

This example shows that the quantities h_2 and θ_2 depend essentially on subtle properties of the coefficients S_{θ_1}. When the power is increased further, new groups of waves are produced, distributed in the form of discrete lines or latitudes on the sphere $\tilde{\omega}_k = 0$, so that we obtain an infinite (with the exception of special singular cases) sequence of thresholds h_2, h_3, ..., and angles θ_2, θ_3, ... The quantities h_3, ..., θ_3, ... are even more sensitive to the structure of the coefficient $S(\theta, \theta')$.

Within the framework of the S-theory, the distributions of the waves with respect to the angles θ are infinitesimally narrow. Actually, there exist physical regions that lead to a smearing of these distributions, foremost among which are the magnetic inhomogeneities of the crystal. At $h < h_2$, where there is one group of pairs, we can easily calculate the nonlinear characteristics of the crystal, namely the high-frequency susceptibilities χ' and χ''. The quantity χ'' is defined as the ratio of the power absorbed in the spin-wave system to the pump power $\omega_p h^2/2$ (see[1]):

$$\chi'' = -\frac{2}{h}\sum \mathrm{Im}(V_k N_k e^{-i\psi_k}). \tag{14a}$$

A similar expression is obtained for the real part of the susceptibility:

$$\chi' = -\frac{2}{h}\sum \mathrm{Re}(V_k N_k e^{-i\psi_k}), \tag{14b}$$

which characterizes the change of the natural frequency of the pump resonator under the influence of the sample.

Using formulas (11) and taking the axial symmetry into account, we obtain explicit expressions for the susceptibility in the important case when only pairs with $\theta_k = \pi/2$ are excited:

$$\chi'' = \frac{2V_1^2}{|S_{11}|}\frac{\sqrt{\zeta^2 - 1}}{\zeta^2}, \quad \chi' = \frac{2V_1^2}{S_{11}}\frac{\zeta^2 - 1}{\zeta^2}, \tag{15}$$

where $\zeta^2 = h^2/h_1^2$ is the excess of the pump power over threshold. Plots of (15) are shown in Fig. 1 for positive S_{11}. In the general case the sign of χ' coincides with the sign of S_{11}. The value of S_{11} was calculated for isotropic ferromagnets in the Appendix. The quantities $S(\theta, \theta')$, and the thresholds and angles of the appearance of the second and succeeding wave groups, and also the behavior of χ' and χ'' at $h > h_2$, were all calculated with a computer.

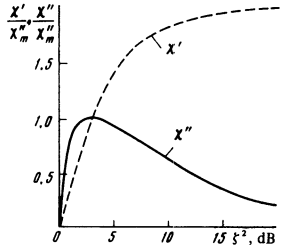

FIG. 1. Theoretical plots of the real (χ') and imaginary (χ'') parts of the nonlinear high-frequency susceptibility vs. the pump power.

2. NUMERICAL EXPERIMENT

The numerical experiment consisted of solving with a computer the system of equations

$$\frac{1}{2}\frac{\partial N_\theta}{\partial t} = N_\theta\left[-\gamma_\theta + hV_\theta \sin\psi_\theta + \sum_{\theta'} S(\theta,\theta')\sin(\psi_\theta - \psi_{\theta'})\right], \quad (16)$$

$$\frac{1}{2}\frac{\partial \psi_\theta}{\partial t} = hV_\theta \cos\psi_\theta + \sum_{\theta'} S(\theta,\theta')\cos(\psi_\theta - \psi_{\theta'}),$$

in which it was already assumed that all the wave pairs lie on the surface $\tilde{\omega}_k = 0$. Solution of these equations yields the correct stationary state and a qualitatively correct description of the transient. In the interval of the angles θ from 0 to $\pi/2$, we chose 21 points $\theta_j = \pi j/40$, j = 0, 1, ..., 20. Doubling the number of points did not affect the result noticeably. We used in the calculation the empirical dependence (10) of the damping γ on the angle θ and realistic values of $S(\theta, \theta')$, calculated with the computer from formulas (A.8) and (A.9) of the Appendix. The calculations were made for different values of the external field H_0, of the magnetization, etc, for YIG samples in the form of a sphere or a disk.

In the solution of (16) we used the following initial conditions, which simulate an equilibrium distribution of the magnons: $N_\theta(0)$ was independent of θ and was smaller by many orders of magnitude than the stationary value of the S-model, and the phase $\psi_\theta(0)$ was random.

Figure 2 shows the calculated dependences of the stationary values of the susceptibilities χ' and χ'' on the pump power for a YIG sphere at $k = 1.3 \times 10^5$ cm^{-1} [1)]. The figure shows also, for comparison, the corresponding χ' and χ'' dependences obtained in the model with one pair with $\theta = \pi/2$ (see (15)), (dashed curves), and the measurement results which are discussed in Sec. 3 below (points). The arrow marks the threshold of production of the second pair, $h_2/h_1 = 2.30$. The angle θ_2 of the production of the second pair lies in the range 40–50°, i.e., it agrees quantitatively with formula (13). It is seen from Fig. 2 that the production of the second pair has a particularly strong effect on the susceptibility χ', which goes through a maximum in the concrete case of YIG, as against a monotonic growth in the single-pair model. It can be shown that the maximum on the χ' curve immediately beyond the threshold of production of the second pair is by far not a general property of the S-theory, and that at other coefficients $S_{kk'}$ the second pair can lead to an even faster growth of χ'.

The numerical experiment has shown that stationary states in the form of one and two pair groups can be distinguished by the character of the transient, namely, the second group of pairs is produced with a certain time delay in the case of a small excess above its threshold h_2. To illustrate this, Fig. 3 shows the time dependence of χ' for a YIG sphere. We see that χ' goes through an oscillatory transient up to h_2 in a time on the order of $\sim 1/V(h - h_1)$. Immediately above the threshold h_2, a quasistationary value of χ', corresponding to the single-pair model, is established within the same time (dashed curve in Fig. 3). The system then varies periodically and arrives after a long time $\sim 1/V(h - h_2)$ at a stationary state in which χ' is smaller than in the quasistationary state. At $h > h_2$ the difference between the quasistationary and stationary values of χ' becomes larger, and the difference between their transient times is smaller.

The numerical experiment made it possible to find the distribution function N_θ for different excesses above threshold. Figure 4 shows N_θ for a YIG sphere.

We note in conclusion that knowledge of the function N_θ may turn out to be useful in the organization and interpretation of new experiments, say, on the scattering of light, neutrons, and sound by parametric spin waves.

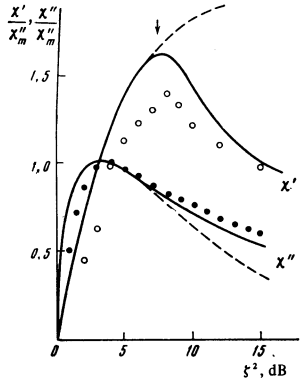

FIG. 2

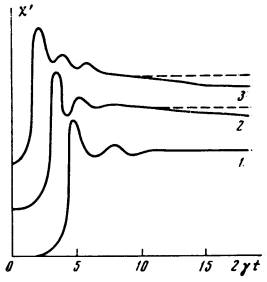

FIG. 3

FIG. 2. Results of computer calculations of the dependences of χ' and χ'' on the pump power for a YIG sphere. The dashed lines show the dependences obtained in the model with one group of pairs with $\theta = \pi/2$. The points are the results of the laboratory experiment. The arrow indicates the excitation threshold of the second group of pairs with $\theta_2 \approx 50°$.

FIG. 3. Time evolution of the real susceptibility χ' at various pump amplitudes for a longitudinally magnetized YIG disk (result of numerical simulation); 1) $h/h_1 = 1.9$, 2) 2.2, 3) 2.5.

3. LABORATORY EXPERIMENT

The measurements were performed in a rectangular TE_{102} resonator with loaded Q = 1800 and a natural frequency $\omega_0 = 9.40$ GHz. We used a procedure with "transmission" and "reflection" measurements. In the "transmission" regime, we registered the power P_{out} passing through the resonator. Its connection with χ'' is

$$\chi'' = \frac{1}{2AQ}\left(\frac{P_{in}}{P_{out}} - 1\right)^{1/2},$$

where

$$A = 2\pi \int_{sample} h^2 dV \Big/ \int_{reson} h^2 dV$$

[1)] Analogous plots for a YIG disk with perpendicular and parallel magnetizations are given in[6].

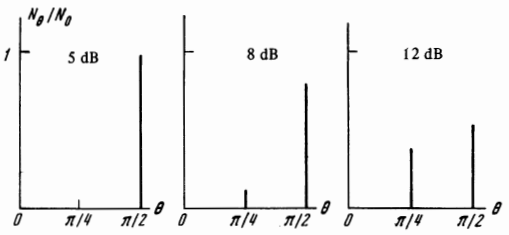

FIG. 4. Pair distribution function at various excesses above threshold.

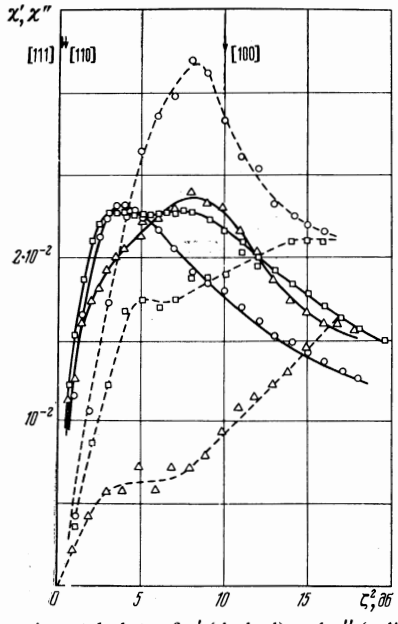

FIG. 5. Experimental plots of χ' (dashed) and χ'' (solid lines) vs. the pump power in a YIG sphere for different crystallographic orientations of the constant magnetic field: ○–$\mathbf{H}_0 \parallel [100]$; △–$\mathbf{H}_0 \parallel [111]$; □–$\mathbf{H}_0 \parallel [110]$. H_0 corresponds to $k = 1.3 \times 10^5$ cm^{-1}.

is the resonator filling factor and P_{in} is the power incident on the resonator; P_{out} and P_{in} are measured in units of the threshold power at the output and input. In the "reflection" regime we measured the power P_{ref} reflected from the resonator; it is connected with χ'' by the relation

$$\chi'' = \frac{1}{2AQ}\frac{(P_{ref}/P_{in})^{1/2}}{1-(P_{ref}/P_{in})^{1/2}},$$

which is valid in the case of critical coupling of the resonator with the waveguide (the reflection coefficient from the unperturbed resonator is equal to zero).

We note that the resonator field h acting on the samples was determined in both cases from the resonator output power, since it is precisely P_{out} and not P_{in} which is proportional to h^2. This has made it possible to take into account automatically the reaction of the sample on the field h, which is appreciable near the threshold even if A is small.

The pump generator was a cw magnetron rated ~ 15 W, modulated by square pulses of 300 μsec duration at a repetition frequency 25 pulses/sec. The pump frequency ω_p could be varied in a small range mechanically, with the aid of a piston and a micrometer screw. This enabled us to compensate for the detuning of the

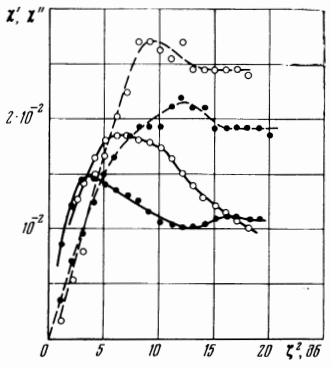

FIG. 6. Experimental plots of χ' (dashed) and χ'' (solid lines) vs. the pump power in a YIG disk: $N_z = 1$ (dark circles), $N_z = 0$ (light circles), $\mathbf{H}_0 \parallel [100]$ and corresponds to $k = 1.3 \times 10^5$ cm^{-1}.

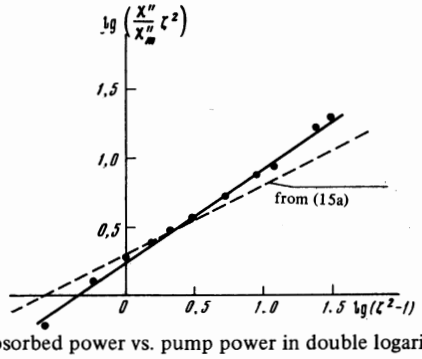

FIG. 7. Absorbed power vs. pump power in double logarithmic scale.

natural resonator frequency and to measure the value of χ' using the formula

$$\chi' = A^{-1}\frac{\omega_0 - \omega}{\omega_0},$$

where ω_0 is the natural frequency of the unperturbed resonator. The absolute error in the measurement of χ' was in this case $\pm 5 \times 10^{-3}$.

Figure 5 shows typical experimental plots of the susceptibilities χ' and χ'' against the power level for a spherical yttrium garnet magnetized along the principal crystallographic directions [100], [110], and [111]. Auto-modulation of χ' and χ'' was observed in the [111] and [110] directions; their threshold is marked by an arrow. The mean values of the susceptibilities are given for these directions.

Figure 6 shows the results of the measurements of $\chi'(\zeta^2)$ and $\chi''(\zeta^2)$ for a disk magnetized parallel and perpendicular to the plane. When the constant magnetic field H_0 varies in the interval corresponding to the excitation of short spin waves, $H_0 < H_c$, the character of the $\chi'(\zeta^2)$ and $\chi''(\zeta^2)$ plots remains essentially unchanged. This pertains in particular to the susceptibility $\chi''(\zeta^2)$. On the other hand, the behavior of $\chi'(\zeta^2)$ is more sensitive to variation of H_0. Plots of $\chi'(\zeta^2)$ and $\chi''(\zeta^2)$ for different fields H_0 were given by us in[6].

4. DISCUSSION OF EXPERIMENTAL RESULTS

1. Dependence of χ'' on the power level. A comparison of the experimental plots of $\chi''(\zeta^2)$ (Fig. 5) with the theoretical plot (Fig. 1) shows them to be in qualitative agreement. There is, however, a quantitative discrepancy; for example, the maximum of $\chi''(\zeta^2)$ is

Table I. Experimental and theoretical values of χ_m''

Sample	$\chi_m''\cdot 10^3$, experiment			$\chi_m''\cdot 10^3$, theory
	$k = 0$	$k = 1.3\cdot 10^5$ cm^{-1}	$k = 2.6\cdot 10^5$ cm^{-1}	
Sphere	23	23	18	27
Disk ∥	20	19	17	34
Disk ⊥	11	15	16	18

reached in the experiment usually when the power exceeds the threshold by 4–6 dB, as against 3 dB in the S-theory. For a quantitative comparison of theory and experiment, we show in Fig. 7 plots of $\chi''(\zeta^2)$ plotted in the coordinates $\log(\chi''\zeta^2)$ and $\log(\zeta^2 - 1)$. The growth of the absorbed power $P_{abs} = \chi''\zeta^2$ can be described by the empirical formula

$$P_{abs} = \text{const}\cdot(\zeta^2 - 1)^{\beta}. \quad (17)$$

The coefficient β for different samples and different experimental conditions (values of H, orientations of the crystal, etc) ranged from 0.6 to 1. A change of β produces a corresponding change in the power level at which χ'' is a maximum; namely, (17) yields $\zeta_m^2 = (1-\beta)^{-1}$. Values of β closer to the theoretical $\beta_{theor} = 0.5$ (see (15)) are observed for the [100] orientation, in which the low-frequency self-oscillations are suppressed. Since the stationary theory does not take the self-oscillations into account, caution must be exercised when formulas (15) are compared with the experimental results obtained for the orientations [111] and [110], where intense self-oscillations are observed. In our subsequent comparison of theory with experiment we shall use mainly the results obtained for the [100] orientation. The difference between the theoretical and experimental plots of $P_{abs}(\zeta^2)$ is not particularly surprising if it is borne in mind that real crystals usually contain a certain amount of inhomogeneities, defects, etc., which are not taken into account in the simple S-theory.

2. Anisotropy of the form of χ''. The maximum value of $\chi''(\zeta^2)$ is given by (15) and (A.11). Substituting in them the concrete values $\omega_M = 2\pi \times 4.9 \times 10^9$ Hz and $\omega_p = 2 \times 9.4 \times 10^9$ Hz, we obtain

$$\chi_m'' = \frac{1}{8\pi}\frac{1}{N_z + 1.18}. \quad (18)$$

Table I lists the experimental and theoretical values of χ_n'' for a sphere ($N_z = 1/3$) and a disk magnetized parallel (disk ∥, $N_z = 0$) and perpendicular (disk ⊥, $N_z = 1$), for the [100] orientation. The values of k given in the table pertain to spin waves with $\theta_k = \pi/2$. The natural frequency of the spin waves and the Hamiltonian coefficients describing three-wave interactions and leading, in particular, to nonlinear damping, are the same within each column. The only difference between samples having different N_z lies in the Hamiltonian coefficients that describe four-wave interaction. Thus, the observed anisotropy of the form of χ_m'' offers evidence that four-wave interaction is responsible for the behavior of the spin waves beyond the threshold. The table shows a reasonable agreement between the conclusions of the S-theory and the experimental results. Special notice should be taken of the regular character of the anisotropy of χ_m'' for a disk. Theory yields for a disk a ratio $\chi_\perp''/\chi_\parallel = 0.53$, and the mean experimental value of this ratio is of the order of 0.75. We note that a reliable numerical comparison of χ_m'' for a disk and a sphere cannot be obtained, owing to the difference between the resonator filling coefficients in the two cases, which we do not know with an accuracy sufficient for the comparison. Nevertheless, the absolute value of χ_m'' for a sphere agrees well with the theoretical value[2)].

3. Real susceptibility χ'. Unlike the imaginary part of the susceptibility χ'', which is characterized mainly by the integral intensity of the pairs, the real part χ' is generally speaking a more sensitive characteristic of the system. It characterizes not only the integral intensity, but also details of the distribution of n_k in k-space, such as self-oscillations etc. This is confirmed by the experimental data of Fig. 5, which shows plots of $\chi'(\zeta^2)$ for the crystallographic directions [100], [110], and [111]. The observed anisotropy of $\chi'(\zeta^2)$ is much larger than that of $\chi''(\zeta^2)$, owing to the self-oscillations that are present in the orientations [110] and [111]. It is interesting that the smallest value of χ' is observed in the [111] direction, where the most intense self-oscillations occur. It follows therefore that the self-oscillations, without influencing strongly the value of χ'', which is correctly predicted by the S-theory, can decrease the real susceptibility χ' by several times. We hope that these peculiarities in the behavior of χ' in the presence of self-oscillations will eventually be explained within the framework of the nonstationary S-theory[11].

We discuss now the behavior of χ' in the stationary regime observed for the [100] orientation. We call attention first to the fact that $\chi' > 0$ for YIG. This agrees with the positive sign of the coefficient S_{11} (see (A.11)), in full accordance with the prediction of the S-theory (Sec. 1). The absolute value of χ', as seen from Figs. 5 and 6, is close to χ'' and exceeds χ'' at large ζ^2. The $\chi'(\zeta^2)$ and $\chi''(\zeta^2)$ plots cross near the maximum of χ'', in agreement with the theoretical relation (15) plotted in Fig. 1. With further increase of $\zeta^2 > 8$ dB, a strong discrepancy between experiment and the theoretical formula (15), which is calculated for one pair with $\theta = \pi/2$, is observed. At an excess of 8 dB there is observed a maximum, and at larger values χ' decreases. Such a behavior of χ' is in full correlation with the results of the numerical experiment, shown in Fig. 2.

Table II gives the experimental and the computer-calculated values of the maximum χ_m' and its position ζ_m^2 for YIG samples of different shapes, as well as the ratios χ_m'/χ_m'', the values of which are more accurate than the absolute values of χ' and χ''. All the values are given for $H_0 = H_c - 100$ Oe and $k = 1.3 \times 10^5$ cm^{-1}.

The satisfactory agreement between theory and experiment confirms the stage-by-stage pair excitation predicted by the S-theory. Namely, at excesses $\zeta^2 < \zeta_m^2$ there is excited in YIG one group of pairs with $\theta_1 = 90°$. The experimentally observed maximum on the $\chi'(\zeta^2)$

[2)] An additional check on the correctness of the S-theory is afforded by a comparison with the experimental results for other cubic crystals. Thus, the experimental value for spherical calcium-bismuth-vanadium garnet (VaBiVIG, $4\pi M \approx 600$ G) is $\chi_m'' \approx 5\times 10^{-3}$, which agrees with the theoretical $\chi_{m\,theor}'' \approx 8\times 10^{-3}$ calculated from formula (18).

Table II

Sample	$\chi'_{m\,exp}\cdot 10^3$	$\chi'_{m\,theor}\cdot 10^3$	$(\chi'_m/\chi''_m)_{exp}$	$(\chi'_m/\chi''_m)_{theor}$	$\zeta^2_{m\,exp}$, dB	$\zeta^2_{m\,theor}$, dB
Sphere	32	42	1,4	1,6	8	8
Disk ∥	27	47	1,4	1,4	8	7
Disk ⊥	22	32	1,5	1,8	12	10

curve is due to the production of a second group of pairs with $\theta_2 \cong 50°$. Beyond the threshold of production of the second group of pairs, we observe also the characteristic behavior theoretically predicted for the transient regime (see Sec. 2). This phenomenon was first observed in[7]. In addition, we have performed a direct experiment that demonstrates threshold excitation of pairs with θ different from 90° (registration of secondary emission in the transverse-pumping channel[8]).

CONCLUSION

As seen from the comparison of the results of the numerical experiment based on the S-theory with the laboratory experiment, the S-theory describes well the behavior of spin waves following their parametric excitation in the stationary case. Let us discuss the role of the factors not accounted for in this theory. These include nonlinear damping of spin waves, which is frequently regarded as the main mechanism that limits the wave amplitude. One of the causes of such damping is heating of the thermal-magnon reservoir by parametric spin waves (PSW)[19]. When this effect is taken into account we have $\gamma = \gamma_0(1 + \alpha\chi''\zeta^2)$, so that

$$\chi'' = (\zeta - 1)/\alpha\zeta^2,$$

which is in fair agreement with experiment if α is suitably chosen ($\alpha \sim 10$). A simple estimate shows, however, that at not too low temperatures we have $\alpha \approx \gamma_0^2/\gamma_T\omega_T$, where ω_T and γ_T are the characteristic frequencies and damping of the thermal magnons. This yields at T ~ 300° a value $\alpha \approx 10^{-3}$—10^{-7}. The remaining nonlinear-damping mechanisms, due to coalescence of parametric spin waves[10], depend strongly on their dispersion law. These mechanisms lead to a damping decrement

$$\gamma = \gamma_0 + \sum \eta^{(3)}_{\mathbf{k}\mathbf{k}'}n_{\mathbf{k}'} + \sum \eta^{(4)}_{\mathbf{k}\mathbf{k}'\mathbf{k}''}n_{\mathbf{k}'}n_{\mathbf{k}''} + \ldots \approx \gamma_0 + \eta^{(3)}N + \eta^{(4)}N^2 + \ldots$$

Each term of this series differs from zero only for a magnetic field smaller than a certain characteristic value H_{3m}, H_{4m}, etc.

The most effective is the mechanism of coalescence of two parametric magnons; for this mechanism

$$\chi''^{(3)} = \frac{2|V_{\mathbf{k}}|^2}{\eta^{(3)}}\frac{\zeta - 1}{\zeta}, \quad \eta^{(3)} \approx \frac{g}{M}\frac{\omega_M^2}{\omega_p}. \tag{19}$$

for the four-magnon process

$$\chi''^{(4)} = \frac{2|V_{\mathbf{k}}|^2}{\sqrt{\gamma_0\eta^{(4)}}}\frac{\sqrt{\zeta - 1}}{\zeta}, \quad \eta^{(4)} \approx \left(\frac{g}{M}\right)^2\frac{\omega_M^2}{\omega_p}. \tag{20}$$

Gottlieb and Suhl[10] have proposed that these nonlinear-damping mechanisms are the main factor that limits the PSW amplitude beyond the threshold. Favoring this hypothesis is the order-of-magnitude agreement between the value of χ'' determined from (19) and the experimental data. Moreover, a jump in the susceptibility χ'' is observed in the field $H = H_{3m}$, at which the mechanism of two-magnon coalescence is turned on[11]. This hypothesis, however, contradicts the experimental data in the following respects:

1. The character of the behavior of χ'', determined from (19), leads to saturation at large ζ, in contradiction to the experiment, in which a decrease of χ'' with increasing ζ is observed.

2. The susceptibility jump in the field $H = H_{3m}$ is equal to $\chi''^{(3)}/\chi''^{(4)}$ and its order of magnitude, as seen from (19) and (20), is

$$\frac{\chi''^{(3)}}{\chi''^{(4)}} \approx \left(\frac{\gamma}{\omega}\right)^{1/2}\frac{\omega}{\omega_M} \approx 10^{-2},$$

whereas the actually observed jump amounts to several times ten per cent.

3. At large excesses ζ^2, there is no jump of χ'' at all in the field H_{3m}.

4. If nonlinear damping imposes the limit, then we should have $\chi' = 0$ (or $\chi' \ll \chi''$). Experiment (see Sec. 4) yields $\chi' \sim \chi''$.

All these experimental facts find a natural explanation of account is taken of the self-consistent parametric pair interaction within the framework of the S-theory. Of all the nonlinear damping mechanisms, only the coalescence of two magnons can compete with their parametric interaction. Therefore when $H > H_{3m}$, when this process is forbidden, nonlinear interaction plays no role and χ'' is determined entirely by the S-theory. In this case $\chi'' \sim |V|^2/|S|$. In the region $H < H_m$, both pair interaction and nonlinear damping are simultaneously active. Then (as already noted earlier[1])

$$\chi'' \approx |V|^2/(S^2 + \eta^{(3)2})^{1/2}.$$

The susceptibility jump is equal to $\sqrt{S^2 + \eta^2}/S$, which is several times ten per cent and agrees with experiment[11] in order of magnitude.

Within the framework of S-theory, as shown above, the detailed behaviors and the values of χ' and χ'' are also naturally explained. As to the absence of a jump in χ'' at small excesses above threshold (less than 6—8 dB), this fact also offers convincing evidence in favor of the S-theory. As already noted, in S-theory, only waves with $\theta = \pi/2$ are excited at $h < h_2$. For these waves, the coefficient characterizing the coalescence of two magnons vanishes identically (see (A.7)).

Thus, in a cubic ferromagnet at pump powers insufficient for the excitation of two (or more) wave groups, the nonlinear damping does not play an important role, even if it is allowed by the conservation laws.

Among the mechanisms that limit the wave amplitudes are also self-oscillations[12]; which are frequently observed in experiment. It follows from our experiments, however, that the presence or absence of self-oscillations does not affect significantly the limitation level, in good agreement with the level predicted by the S-theory. This suggests that self-oscillations are

not the mechanism that limits the wave amplitude. Moreover, the very mechanism whereby the self-oscillations are produced is not clear. In addition to the inertia mechanism proposed in[12], there may exist mechanisms that do not go outside the framework of the nonstationary S-theory. The coefficients $S_{kk'}$ and $T_{kk'}$ of the wave interaction Hamiltonian can be such that stable stationary states exist in the system[1]. The numerical experiment performed for this case results in establishment of self-oscillations having properties similar to those observed in experiment. On the whole, the problem of self-oscillations remains open. In particular, the cause of the strong anisotropy of the properties of the self-oscillations in almost-isotropic cubic ferromagnets remains unclear. Another important problem is the influence of magnetic inhomogeneities on the properties of the parametrically-excited waves.

In conclusion, the authors thank A. G. Gurevich for numerous useful remarks.

APPENDIX

We write down the expression for the energy of an isotropic ferromagnet in the form

$$W = -HM_z(0) + \frac{\omega_{ex}}{2gM_0}\sum_{\mathbf{k}}\mathbf{M}(\mathbf{k})\mathbf{M}^*(\mathbf{k})(lk)^2 + \frac{\omega_M}{2gM_0}\left\{\sum_{\mathbf{k}}\frac{(\mathbf{kM}(\mathbf{k}))(\mathbf{kM}^*(\mathbf{k}))}{k^2} - [N_xM_x^2(0) + N_yM_y^2(0) + N_zM_z^2(0)]\right\}, \quad (A.1)$$

$$\mathbf{M}(\mathbf{k}) = \sum_{\mathbf{k}}\mathbf{M}(\mathbf{r})e^{-i\mathbf{kr}}, \quad (A.2)$$

where g is the gyromagnetic ratio, ω_{ex}/g is the exchange field, $\omega_M = 4\pi gM_0$, and $N_x + N_y + N_z = 1$ are the demagnetizing factors. We change over in (A.1) to the canonical variables a_k and a_k^*, using the formulas

$$M_+(\mathbf{k}) = \sqrt{2gM_0}\left\{a_{\mathbf{k}} - \frac{g}{2M_0}\sum_{\mathbf{k}_1,\mathbf{k}_2,\mathbf{k}_3}a_1a_2a_3^*\Delta(\mathbf{k}_1+\mathbf{k}_2-\mathbf{k}_3-\mathbf{k})\right\},$$
$$M_z(\mathbf{k}) = M_0\Delta(\mathbf{k}) - g\sum_{1,2}a_1a_2^*\Delta(\mathbf{k}_1-\mathbf{k}_2-\mathbf{k}), \quad (A.3)$$

where $M_+ = M_x + iM_y$, $\Delta(\mathbf{k})$ is the Kronecker symbol: $\Delta(0) = 1$, $a_1 \equiv a_{\mathbf{k}}$, etc. The ferromagnet energy (A.1) expressed in terms of the canonical variables becomes the Hamiltonian

$$H = \sum_{\mathbf{k}}A_{\mathbf{k}}a_{\mathbf{k}}a_{\mathbf{k}}^* + \tfrac{1}{2}\sum_{\mathbf{k}}(B_{\mathbf{k}}^*a_{\mathbf{k}}a_{-\mathbf{k}} + B_{\mathbf{k}}a_{\mathbf{k}}^*a_{-\mathbf{k}}^*) \quad (A.4)$$
$$+ \sum_{1,23}\{V_{1,23}^*a_1^*a_2a_3 + \text{c.c.}\} + \tfrac{1}{2}\sum_{12,34}W_{12,34}a_1^*a_2^*a_3a_4\Delta(\mathbf{k}_1+\mathbf{k}_2-\mathbf{k}_3-\mathbf{k}_4)$$
$$+ \tfrac{1}{4}\sum_{1,234}\{G_{1,234}a_1a_2^*a_3^*a_4^*\Delta(\mathbf{k}_1-\mathbf{k}_2-\mathbf{k}_3-\mathbf{k}_4) + \text{c.c.}\},$$

where ($k_+ = k_x + ik_y$)

$$A_{\mathbf{k}} = \omega_H - N_z\omega_M + \omega_{ex}(lk)^2 + |B_{\mathbf{k}}|,\quad B_{\mathbf{k}} = \omega_M k_+^2/2k^2,$$
$$A_0 = \omega_H - N_z\omega_M + \tfrac{1}{2}(N_x+N_y)M_0,\quad B_0 = \tfrac{1}{2}\omega_M(N_y-N_x),$$
$$V_{1,23} = \tfrac{1}{2}(V_2+V_3),\quad V_{\mathbf{k}} = -\omega_M(g/2M)^{1/2}k_zk_+/k^2,$$
$$W_{12,34} = E_{12}+E_{34}+\tfrac{1}{4}(C_{13}+C_{14}+C_{23}+C_{24}) - \tfrac{1}{4}(D_1+D_2+D_3+D_4),$$
$$E_{\mathbf{kk}'} = -\frac{g}{2M}\omega_{ex}l^2\mathbf{kk}',\quad C_{\mathbf{kk}'} \equiv C(\mathbf{k}-\mathbf{k}'),\quad C(\mathbf{k}) = \frac{g}{M}\omega_M\frac{k_z^2}{k^2},$$
$$C(0) = \frac{g}{M}\omega_MN_z,\qquad D_{\mathbf{k}} = \frac{g}{2M}\omega_M\frac{|k_+|^2}{k^2} = \frac{g}{M}|B_{\mathbf{k}}|,$$
$$G_{1,234} = -\frac{1}{3}\frac{g}{M}(B_2+B_3+B_4) \quad (A.5)$$

We now carry out a canonical (u, v) transformation that diagonalizes the quadratic part of H:

$$a_{\mathbf{k}} = u_{\mathbf{k}}b_{\mathbf{k}} + v_{\mathbf{k}}b_{-\mathbf{k}}^*,$$

where

$$u_{\mathbf{k}} = \sqrt{\frac{A_{\mathbf{k}}+\omega_{\mathbf{k}}}{2\omega_{\mathbf{k}}}},\quad v_{\mathbf{k}} = -\frac{B_{\mathbf{k}}}{|B_{\mathbf{k}}|}\sqrt{\frac{A_{\mathbf{k}}-\omega_{\mathbf{k}}}{2\omega_{\mathbf{k}}}},\quad \omega_{\mathbf{k}}^2 = A_{\mathbf{k}}^2 - |B_{\mathbf{k}}|^2.$$

In terms of the variables b_k we have

$$H = \sum_{\mathbf{k}}\omega_{\mathbf{k}}b_{\mathbf{k}}b_{\mathbf{k}}^* + \sum_{1,23}\{V_{1,23}^*b_1^*b_2b_3\Delta(\mathbf{k}_1-\mathbf{k}_2-\mathbf{k}_3) + \tfrac{1}{3}U_{123}^*b_1b_2b_3\cdot$$
$$\cdot\Delta(\mathbf{k}_1+\mathbf{k}_2+\mathbf{k}_3) + \text{c.c.}\} + \tfrac{1}{2}\sum_{12,34}W_{12,34}b_1^*b_2^*b_3b_4\Delta(\mathbf{k}_1+\mathbf{k}_2-\mathbf{k}_3-\mathbf{k}_4) + \ldots; \quad (A.6)$$

$$V_{1,23} = \tfrac{1}{2}\{(V_2+V_3)u_1u_2u_3 + (V_2^*+V_3^*)v_1^*v_2v_3 + (V_1v_1^* + V_1^*v_1)(u_2v_3+v_2u_3) + v_1^*(V_2u_2v_3 + V_3u_3v_2) + u_1(V_2^*v_2u_3 + V_3^*v_3u_2)\},$$

$$U_{123} = \tfrac{1}{2}\{V_1u_1(v_2u_3+v_3u_2) + V_2u_2(v_3u_1+v_1u_3) + V_3u_3(v_1u_2+v_2u_1)\}. \quad (A.7)$$

The general expression for W is even more cumbersome. We write it out for the case of interest to us:

$$S_W(\mathbf{k},\mathbf{k}') \equiv W_{\mathbf{k},-\mathbf{k};\mathbf{k}',-\mathbf{k}'}$$
$$= W_1(u_{\mathbf{k}}^2u_{\mathbf{k}'}^2 + v_{\mathbf{k}}^2v_{\mathbf{k}'}^{*2}) + 4W_2u_{\mathbf{k}}u_{\mathbf{k}}v_{\mathbf{k}}v_{\mathbf{k}'}^* - \frac{g}{2M}\{v_{\mathbf{k}}u_{\mathbf{k}'}(u_{\mathbf{k}}u_{\mathbf{k}'}[B_{\mathbf{k}}^* + 2B_{\mathbf{k}'}^*]$$
$$+ v_{\mathbf{k}}v_{\mathbf{k}'}^*(B_{\mathbf{k}'}^* + 2B_{\mathbf{k}}^*)) + v_{\mathbf{k}'}^*u_{\mathbf{k}}[u_{\mathbf{k}}u_{\mathbf{k}'}(2B_{\mathbf{k}}+B_{\mathbf{k}'}) + (2B_{\mathbf{k}'}+B_{\mathbf{k}})v_{\mathbf{k}}v_{\mathbf{k}'}^*]\}, \quad (A.8)$$

$$W_1 = \frac{g}{2M}\{\omega_{ex}(lk)^2 - \omega_M\},\quad W_2 = \frac{g}{2M}\omega_M(N_z-1).$$

We note that in (A.6) we did not write out the fourth-order terms of the type $1 \to 3$ and $0 \to 4$, since they do not describe the interactions of the parametric spin waves with one another. In addition to terms of the type $2 \to 2$, an important contribution is made to this interaction by those terms of the Hamiltonian (A.6) which are of third order in second-order perturbation theory. It is convenient to account for this contribution by performing the transformation (A1, 1) of[4] into new canonical variables c_k, chosen such that the resultant Hamiltonian has no triple terms, i.e., it has the form (1). The general expression for $T_{k_1k_2k_3k_4}$ is given in[4]. We are interested only in its particular case when $\mathbf{k}_2 = -\mathbf{k}_1$ and $\mathbf{k}_4 = -\mathbf{k}_3$:

$$S(\mathbf{k}_1,\mathbf{k}_2) = S_W(\mathbf{k}_1,\mathbf{k}_2)$$
$$- 2\frac{\tilde{U}_{01\bar{1}}^*\tilde{U}_{02\bar{2}}}{\omega_0+\omega_p} - 2\,\mathrm{Re}\frac{\tilde{V}_{0.1\bar{1}}^*\tilde{V}_{0.2\bar{2}}}{\omega_0-\omega_p} - 4\frac{\tilde{V}_{1.23}\tilde{V}_{\bar{2}.\bar{1}3}^*}{\omega_3} - 4\frac{\tilde{V}_{1.\bar{2}4}\tilde{V}_{\bar{2}.\bar{1}4}^*}{\omega_4}, \quad (A.9)$$

where $\mathbf{k}_3 \equiv \mathbf{k}_1 - \mathbf{k}_2$, $\mathbf{k}_4 \equiv \mathbf{k}_1 + \mathbf{k}_2$, the index $\bar{2}$ corresponding to $-\mathbf{k}_2$, and $\omega_0^2 = A_0^2 - |B_0|^2$ is the frequency of the homogeneous magnetization precession. The second and third terms of (A.9) are due to the interaction of pairs with $\mathbf{k}_1$ and $\mathbf{k}_2$ via "virtual" homogeneous precession, and the last two terms correspond to interaction via "virtual" spin waves with $\mathbf{k} = \mathbf{k}_1 + \mathbf{k}_2$.

Expressions (A.6), (A.8), (A.9), (A.7), and (8) were used by us for computer calculation of the coefficients $S_{kk'}$ of the diagonal (in terms of the pairs) spin-wave interaction Hamiltonian in YIG.

In the important particular case $\theta_1 = \theta_2 = \pi/2$, the third-order terms make no contribution to $S_{kk'}$ and

$$S(\varphi) = \frac{g}{2M}\{\omega_{ex}(lk)^2 - \omega_M)(u^4 + v^4e^{4i\varphi}) + 4\omega_Mu^2v^2e^{2i\varphi}(N_z-1)$$

$$+\omega_M u|v|[u^2+2(u^2+v^2)e^{2i\varphi}+v^2e^{4i\varphi}]\}, \qquad \text{(A.10)}$$

where $\varphi \equiv \varphi_1 - \varphi_2$

$$u^2=\frac{1}{2}\left[\sqrt{\frac{\omega_p^2+\omega_M^2}{\omega_p^2}}+1\right], \quad v^2=\frac{1}{2}\left[\sqrt{\frac{\omega_p^2+\omega_M^2}{\omega_p^2}}-1\right].$$

Of particular interest is

$$S_{11}=\frac{1}{2\pi}\int_0^{2\pi}S(\varphi)e^{-2i\varphi}d\varphi,$$

which is equal to

$$S_{11}=\frac{g}{2M}\left(\frac{\omega_M}{\omega_p}\right)^2\{\omega_M(N_z-1)+\sqrt{\omega_p^2+\omega_M^2}\}. \qquad \text{(A.11)}$$

[1]V. E. Zakharov, V. S. L'vov, and S. S. Starobinets, Zh. Eksp. Teor. Fiz. **59,** 1200 (1970) [Sov. Phys.-JETP **32,** 656 (1971)].

[2]V. E. Zakharov and V. S. L'vov, Zh. Eksp. Teor. Fiz. **60,** 2066 (1971) [Sov. Phys.-JETP **33,** 1113 (1971)].

[3]V. E. Zakharov, V. S. L'vov, and S. S. Starobinets, Fiz. Tverd. Tela **11,** 2922 (1969) [Sov. Phys.-Solid State **11,** 000 (1970)].

[4]R. Damon, in: Magnetism, ed. by Rado and Suhl, Vol. 1, 1963.

[5]Yu. M. Yakovlev, Yu. N. Burdin, Yu. R. Shil'nikov, and T. N. Bushueva, Fiz. Tverd. Tela **12,** 3059 (1970) [Sov. Phys.-Solid State **12,** 000 (1971)].

[6]V. V. Zautkin, V. E. Zakharov, V. S. L'vov, S. L. Musher, and S. S. Starobinets, Nuc. Phys. Inst., Preprint IYaF 52-71, 1971.

[7]G. A. Petrakovskiĭ and V. N. Berzhanskiĭ, Zh. Eksp. Teor. Fiz. Pis'ma Red. **12,** 429 (1970) [JETP Lett. **12,** 298 (1970)].

[8]V. V. Zautkin, V. S. L'vov, S. L. Musher, and S. S. Starobinets, Zh. Eksp. Teor. Fiz. Pis'ma Red. **14,** 310 (1971) [JETP Lett. **14,** 206 (1970)].

[9]E. Schlömann, J. Appl. Phys. **33,** 527 (1962).

[10]P. Gottlieb and H. Suhl, J. Appl. Phys. **33,** 1508 (1962).

[11]T. S. Hartwick, E. R. Peressini, and M. T. Weiss, J. Appl. Phys. **32,** 2235 (1961).

[12]Ya. A. Monosov, Nelineinyĭ ferromagnitnyĭ rezonans (Nonlinear Ferromagnetic Resonance), Nauka, 1971.

Translated by J. G. Adashko
205